

# Improving the Abel transform inversion using bending angles from FORMOSAT-3/COSMIC

Angela Aragon-Angel · Manuel Hernandez-Pajares ·  
J. Miguel Juan Zornoza · Jaime Sanz Subirana

Received: 4 February 2009 / Accepted: 10 October 2009  
© Springer-Verlag 2009

**Abstract** The FORMOSAT-3/COSMIC satellite constellation has become an important tool toward providing global remote sensing data for sounding of the atmosphere of the earth and the ionosphere in particular. In this study, the electron density profiles are derived using the Abel transform inversion. Some drawbacks of this transform in LEO GPS sounding can be overcome by considering the separability concept: horizontal gradients of vertical total electron content (VTEC) information are incorporated by the inversion method, providing more accurate electron density determinations. The novelty presented in this paper with respect to previous works is the use of the phase change between the GPS transmitter and the LEO receiver as the main observable instead of the ionospheric combination of carrier phase observables for the implementation of separability in the inversion process. Some of the characteristics of the method when applied to the excess phase are discussed. The results obtained show the equivalence of both approaches but the method exposed in this work has the potentiality to be applied to the neutral atmosphere. Recent FORMOSAT-3/COSMIC data have been processed with both the classical Abel inversion and the separability approach and evaluated versus colocated ionosonde data.

**Keywords** GPS radio occultation · Ionosphere · Electron density · Abel transform · Separability · FORMOSAT-3/COSMIC

## Introduction

The Abel transform is a frequently used radio occultation inversion technique which in the ionospheric context, allows retrieving electron densities as a function of height from STEC (Slant Total Electron Content) measurements derived from carrier phase observations. The GPS radio occultation technique is based on precise carrier dual-frequency phase measurements (L-band) of a GPS receiver onboard a Low Earth Orbit satellite (LEO) tracking a rising or setting GPS satellite behind the limb of the earth (Schreiner et al. 1999). When combining such measurements with the information from the positions and velocities of GPS and LEO satellites, it is possible to derive the phase path change due to the atmosphere during an occultation event that subsequently can be converted into bending angles. From these, we can obtain information about the vertical refraction index by means of inversion techniques, which can then be converted into ionospheric vertical electron density profiles and/or neutral atmospheric profiles. One of the basic assumptions in the classical approach of the Abel inversion is to assume the spherical symmetry of the electron density field in the vicinity of an occultation. However, in practice, the footprint of an occultation generally covers wide regions of thousands of kilometers in length that may show significant ionospheric variability (Hernandez-Pajares et al. 2009); therefore, this hypothesis cannot be guaranteed. Indeed, inhomogeneous electron density in the horizontal direction for a given occultation is believed to be one of the main sources of error when using the Abel inversion. In order to correct the error due to the spherical symmetry assumption, the separability concept in Hernandez-Pajares et al. (2000) is introduced and applied. This implies that the electron density can be expressed by a combination of externally

---

A. Aragon-Angel (✉) · M. Hernandez-Pajares ·  
J. M. J. Zornoza · J. S. Subirana  
Research Group of Astronomy and Geomatics,  
Technical University of Catalonia, Module C3,  
Room 210, 08034 Barcelona, Spain  
e-mail: angela@ma4.upc.edu

derived vertical total electron content (VTEC) data, which assumes the horizontal dependency, and a shape function that in turn assumes the height dependency that is common to all the observations for a given occultation. Note that the slab thickness remains constant near the occultation due to the separability hypothesis instead of the density as is the case of the spherical symmetry. This technique was successfully applied to the linear combination of the GPS carrier phases  $L_1$  and  $L_2$ ,  $LI = L_1 - L_2$ , which is a geometric free observable that depends only on the ionospheric delay, phase ambiguity, instrumental bias and wind-up. The result was an improvement of about 40% in RMS when comparing frequencies of the  $F2$  layer peak with ionosonde data and the classical Abel inversion (Hernandez-Pajares et al. 2000; Garcia-Fernandez 2004). The main advantage of the technique developed in Hernandez-Pajares et al. (2000) is its simple computation. Nevertheless, the potential influence of the different signal paths between  $L_1$  and  $L_2$  was neglected. Regarding this aspect, this paper shows that it is not a problem for inversion at ionospheric heights. An alternative to inverting the profile, which overcomes this disadvantage, is to use the bending angle of the signal ( $\alpha$ ) as the main input data. The implementation of separability when using the bending angle is not immediate and was, actually, one of the goals of this work. In this sense, the separability approach has been applied to measured  $\alpha_1$  ( $L_1$  bending angle), instead of the LI combination as reported in previous work. Additionally, this approach could also be translated to tropospheric profile retrievals. The performance of this implementation has been studied using FORMOSAT-3/COSMIC data. The successful deployment of the FORMOSAT-3/COSMIC constellation (Lei et al. 2007), which started in April 2006, provides sets of occultation data distributed globally and almost uniformly, thus overcoming two limitations of previous LEO missions: sparsity and scarcity of occultation data. For instance, the GPS/MET mission provided about 250 (Hajj and Romans 1998), CHAMP and SAC-C missions provided more than 400 (Hajj et al. 2004) daily occultations while FORMOSAT-3/COSMIC yields about 2000 (Anthes et al. 2008).

### Clock calibration

For this study, the basic observable used in analyzing occultations is the signal phase change between GPS transmitter and LEO receiver as the signal travels through the atmosphere. It is possible to derive the extra phase change induced by the atmosphere and then, from it, obtain the excess Doppler shift  $f_d$  (in meters) as the departure from the straight line propagation

$$f_d = \frac{d}{dt}(L - |\vec{r}_R - \vec{r}_T|) \quad (1)$$

where  $\vec{r}_R$  and  $\vec{r}_T$  stand for the receiver and transmitter positions (Hajj and Romans 1998). The Doppler shift at the operating frequency  $f_T$  (in meters) can be also expressed using

$$\begin{aligned} \frac{dL}{dt} &= -\frac{f_T}{c}(\vec{v}_T \cdot \hat{e}_T + \vec{v}_R \cdot \hat{e}_R) \\ &= -\frac{f_T}{c}(v_T^r \cos \phi_T + v_T^\theta \sin \phi_T + v_R^r \cos \phi_R - v_R^\theta \cos \phi_R) \end{aligned} \quad (2)$$

where  $c$  is the speed of light,  $\vec{v}_T$  and  $\vec{v}_R$  are the transmitter and receiver velocities, and  $\hat{e}_T$  and  $\hat{e}_R$  are the unit vectors tangent to the optical ray path at the transmitter and receiver positions. The symbols  $\phi_T$  and  $\phi_R$  denote the angles between  $\vec{v}_T$  and  $\hat{e}_T$  and  $\vec{v}_R$  and  $\hat{e}_R$ , respectively,  $v_T^r$  and  $v_T^\theta$  represent the radial and transversal components of the transmitting spacecraft velocity and  $v_R^r$  and  $v_R^\theta$  are the respective velocity values for the LEO receiver. This extra Doppler shift is used to derive the atmospheric bending as a function of the impact parameter i.e., the closest point to the earth center along the optical ray path (Hajj and Romans 1998). In order to obtain accurate radio occultation inversions, the FORMOSAT-3/COSMIC and GPS clock errors need to be removed from the raw observables. Otherwise, the clock drifts can contribute significantly to the excess Doppler. Figure 1 shows an example of a non-calibrated excess Doppler, calculated from (1). Indeed, the most relevant terms when modeling the carrier phase observable  $L_i^j$  between a LEO receiver ( $i$ ) and the GPS transmitter ( $j$ ) for an ionospheric occultation are

$$L_i^j = |\vec{r}^j - \vec{r}_i| + c(T_i - T^j) + \text{rel}_i^j - \text{Ion}_i^j + B_i^j \quad (3)$$

where  $T_i$ , and  $T^j$  stand for the clock offsets of the LEO and the GPS satellite from GPS time,  $\text{rel}_i^j$  is the relativistic effect,  $\text{Ion}_i^j$  is the ionospheric delay and  $B_i^j$  is the phase ambiguity. When taking the time derivatives of this expression, the first two terms are the most significant, i.e.

$$\frac{dL_i^j}{dt} = \frac{d|\vec{r}^j - \vec{r}_i|}{dt} + c \frac{d(T_i - T^j)}{dt} \quad (4)$$

If the clock errors are not properly treated, the main contribution could come from the last term in (4).

It follows from (4) that it is necessary to remove the geometrical effects due to the motion of the satellites and properly calibrate the transmitter and receiver clocks. This is accomplished by double differencing (noted as DD) the phase measurements from the onboard GPS receiver and a fiducial ground receiver (Wickert et al. 2001). Applying double differencing to any given occultation requires a global ground network. Other authors apply space-based

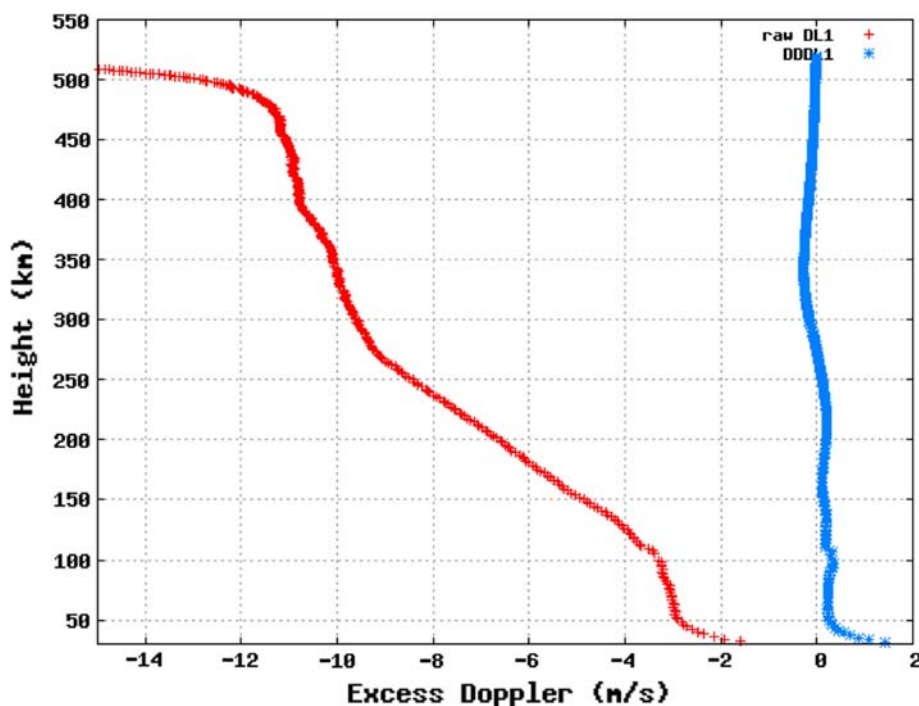


**Fig. 1** FORMOSAT-3/COSMIC occultation on Jan 6, 2007, PRN 17, LEO I241, 04 h 25 min UT: raw  $L_1$  excess Doppler (without removing clock drifts) derived from FORMOSAT-3/COSMIC observables versus doubled differenced  $L_1$  excess Doppler (DDD1). The unrealistic values of the raw  $L_1$  excess Doppler, which are a result of the clock drifts, can readily be seen. For graphical purposes, the excess Doppler values are denoted by DL1 and DL2 for the excess

single differencing (Wickert et al. 2002) instead of double differencing. For instance, in the case of FORMOSAT-3/COSMIC constellation, UCAR/CDAAC currently use single differences with solved GPS clocks from prior 30 s that, consequently, do not require ground station data as such (Schreiner et al. 2008).

For this study, to remove the receiver and transmitter clock drifts, we use the fact that the Doppler shift can be deduced to be proportional to the electron density gradient and the inverse of the square frequency (see Appendix) given that the GPS frequencies are considerably larger than the plasma frequency  $f_p = 20$  MHz. Figure 2 shows the double difference excess Doppler for  $L_1$ ,  $L_2$  and the ionospheric free combination  $L_c$ . It is readily seen that the excess phases  $L_1$  and  $L_2$  are inversely proportional to the frequency (the values for  $L_2$  excess Doppler have been scaled by the factor  $f_2^2/f_1^2$ ). This implies that the ray paths of  $L_1$  and  $L_2$  signals are basically the same:

- The bending angle or excess phase rate of both signals are proportional to the inverse square frequency (as the ionospheric effect in a straight line propagation).
- The trajectory of  $L_1$  and  $L_2$  signals is different (because of the different curvature) but this difference in trajectories has not a relevant effect in the excess

Doppler in  $L_2$ , etc. Notice that our naming convention for FORMOSAT-3/COSMIC LEOs is that followed in the satellite orbit-clock sp3-files provided by UCAR (<http://cosmic-io.cosmic.ucar.edu/cdaac/login/>), e.g., in I2XY. The X stands for the spacecraft number ranging from 1–6, and Y is the antenna code ranging from 0 to 3. GPS satellites are identified by the PRN (Pseudo Random Number)

phase rate. Notice that if the trajectories were different enough, they should not cancel out since the rays would be crossing through different electron densities. In our case, since  $DDDL_c = 0$ , it implies that the trajectories, in spite of being different, they are not that different as to have influence in the measurement of the curvature.

Taking advantage of the proportional relationship between the excess phases  $L_1$  and  $L_2$ , the ionospheric free combination  $L_c$  can be used to obtain an observable with no bending (see  $DDDL_c$  in Fig. 2) and, in the undifferenced form ( $DL_c$ ), this particular observable would depend only on the clock drift and  $\frac{d}{dt}|\vec{r}^j - \vec{r}_i|$ . Therefore, it removes the clock drifts when subtracted from raw excess Doppler  $L_1$ . Figure 3 shows an example of the equivalence of clock drift removal at ionospheric heights between the double differenced excess phase of  $L_1$  and the new combination with no bending. Note that not only the observables are equivalent, but their noise level is compatible. The noticeable discrepancies at bottom heights reflect the tropospheric delay signature, which affects only the double difference method at heights corresponding to troposphere (when subtracting  $DL_c$ , the tropospheric delays are also canceled out).

**Fig. 2** FORMOSAT-3/ COSMIC occultation on Jan 8, 2007, PRN 13, LEO 1241, 04 h 32 min UT: Equivalence of double difference  $L_1$  and  $L_2$  phase rate excess (DDDL1 and DDDL2, respectively) for the occultation. The  $L_2$  rates were scaled to  $L_1$  frequency. The double difference (between GPS transmitter under occultation and a standard one, and between two COSMIC receivers) of  $L_c$  phase rate excess (DD[DLc]) is basically vertically distributed

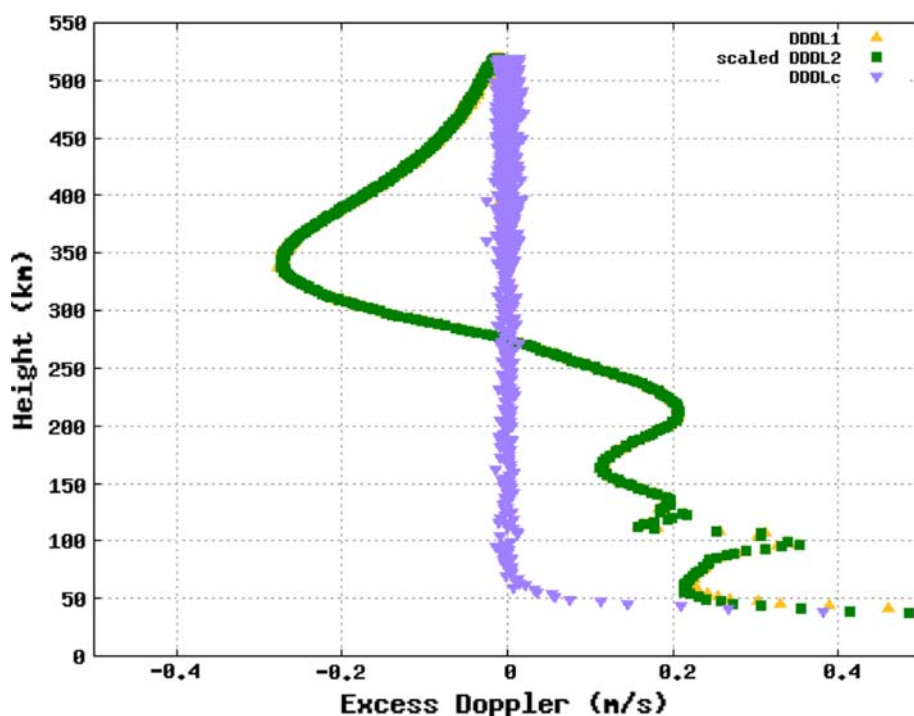
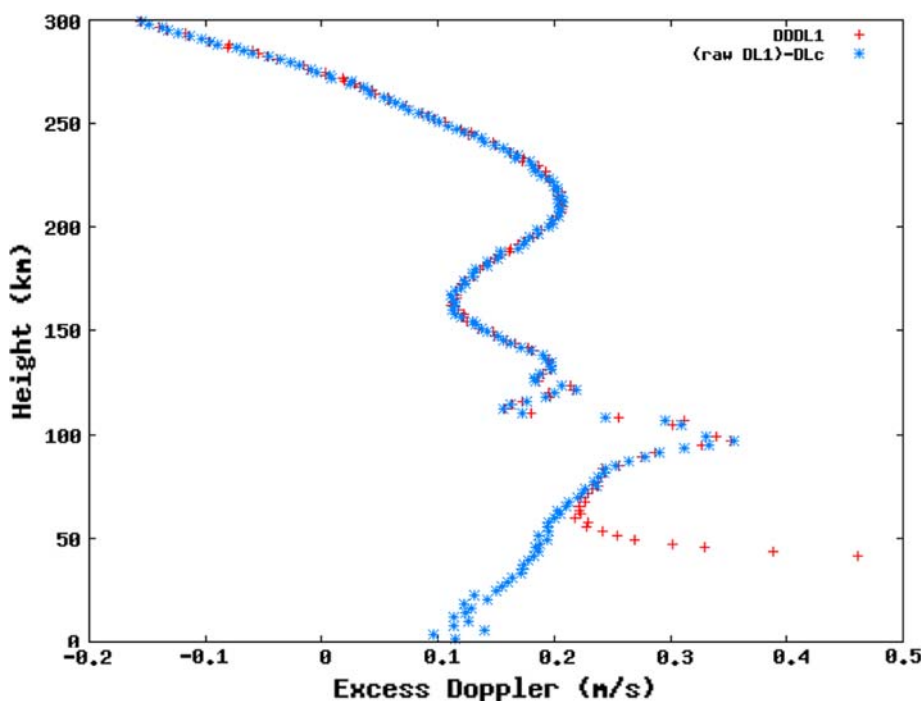


**Fig. 3** FORMOSAT-3/ COSMIC occultation for Jan 8, 2007, PRN 13, LEO 1241, 04 h 32 min UT: Equivalence of clock calibration strategies: The red cross symbols,  $L_1$  excess Doppler (represented by DL1) without clock drifts by double differencing (noted with DD) using a second pair of non-occluding LEO and GPS satellites. The blue asterisk symbols,  $L_1$  excess Doppler without clock drifts by subtracting  $L_c$  observable to  $L_1$  (represented by (raw DL1)-DLc)



The clock calibration method used in this work is valid for ionospheric radio occultation processing. With this approach, no extra GPS transmitters or LEO receivers are needed in addition to those involved in the radio occultation event when calibrating the clocks. Consequently, more occultations can be inverted with less data processing and computational load. However, double differencing will be required for tropospheric retrievals.

### Separability and bending angle

As mentioned earlier, the classical Abel transform assumes the spherical symmetry in the vicinity of an occultation when retrieving electron density profiles. In order to reduce the error due to this underlying assumption, Hernandez-Pajares et al. (2000) developed the separability concept that helps mitigating this drawback considering that the

electron density  $N_e$  can be expressed as a function of VTEC and the shape function  $F$  as

$$N_e(\lambda, \varphi, h) = \text{VTEC}(\lambda, \varphi) \cdot F(h) \quad (5)$$

The symbols  $\lambda$  and  $\varphi$  denote longitude and latitude, and  $h$  is the height. Information for VTEC is externally provided by either a model or real data. Therefore, the shape function becomes the new unknown to be solved. Notice that the hypothesis of sharing the same shape function in the neighboring area of the occultation is less restrictive than sharing the same electron density (as the spherical symmetry assumption would imply). In this paper, the VTEC information has been spatially/temporally interpolated at each location following the procedure by Schaer et al. (1998) using the ionospheric product provided in IONEX (IONosphere map EXchange) format, and computed for the International GNSS Service (IGS) at the Technical University of Catalonia. The implementation of (5) in the equations of the inversion problem with bending angles as data input is not straightforward because the relationship between refractive index and electron density is not proportional. In the Appendix, we derive a linear relationship that can be applied in a discretized way, considering a concentric layered atmosphere with radius  $h_i$  and corresponding refractive indices. The final bending angle  $\alpha$  is obtained:

$$\alpha = \frac{1}{2\varepsilon_0 m (2\pi f)^2} \sum \text{VTEC}(\lambda_i, \varphi_i) \Delta F(h_i) \tan \phi_i \quad (6)$$

where  $(\lambda_i, \varphi_i)$  are the geographic coordinates at the intersection of the LOS (Line Of Sight) vector with the  $i$ th layer. The radius of such a layer is derived from the impact parameter of the corresponding observation. The thickness of consecutive layers can range from about 0.1 to 4 km, depending on the observation rate and satellite orbit. Therefore, to assume that the ionospheric effect is constant within these shell thicknesses is not critical.

One way to confirm the validity of the separability hypothesis is to compare the shape functions corresponding to collocated occultations. Such example is provided below. Figure 4 shows a map of VTEC values for January 8, 2007 of the Ascension Island region. Co-located electron density profiles from FORMOSAT-3/COSMIC occultations are also marked (12 h UT, 13 h LT approximately).

The corresponding electron density profiles to these occultations are shown in Fig. 5. These profiles have been derived using separability. Note that such density profiles follow the VTEC behavior, i.e., higher VTEC values lead to higher electron densities. Discrepancies among the profile shapes are significant.

Nevertheless, in Fig. 6, when considering the shape functions corresponding to these profiles, the shapes become closer in value.

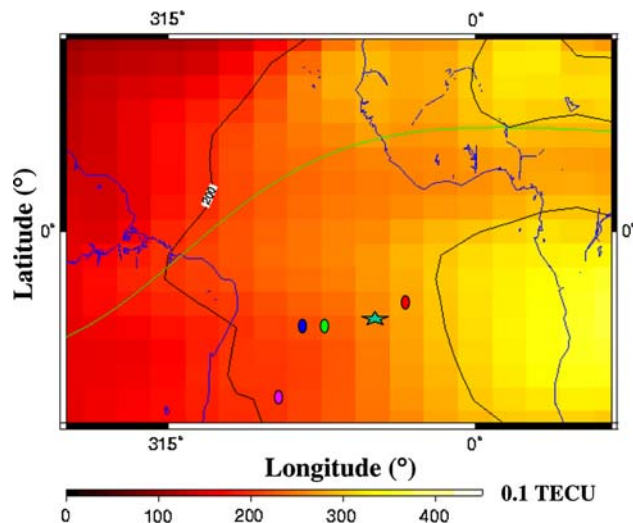


**Fig. 4** VTEC values and collocated vertical electron density profiles for the Ascension Island region. The *green star* is located at Ascension Island referring to observation epoch 12 h UT (approx. 13 h LT) for January 8, 2007. The color code for the occultations (*colored circles*) follows the same pattern used in Figs. 5 and 6. The geomagnetic equator is depicted by the *green line*

This fact can be interpreted as the horizontal variations of the shape functions are lower than the horizontal variations of the electron densities, confirming the suitability of the separability hypothesis. Actually, as it can be seen later, separability significantly helps mitigate the error in the frequency peak estimation but not the error in height.

## Scenario

The period for analysis of FORMOSAT-3/COSMIC observations is January 6–15, 2007, during which the solar cycle level was at a minimum. The Kp index, which indicates global geomagnetic activities, was low for the chosen data period (Kp less than 3, which means low geomagnetic activity). In order to validate the retrieved electron density profiles, a comparison with ionosonde measurements has been performed for critical frequencies and heights of the  $F_2$  layer,  $f_oF_2$  and  $hmF_2$ , and for critical frequencies of the  $E$  layer,  $f_oE$ . The reference data were downloaded from the Space Physics Interactive Data Resource (SPIDR) website (<http://spidr2.ngdc.noaa.gov/spidr/>). In order to filter and rule out doubtful comparisons, the slab thickness parameter  $\tau$  has been considered. It is calculated for each vertical electron density profile as a ratio of the VTEC and the electron density at the  $F_2$  layer peak ( $NmF_2$ ),

$$\tau = \frac{\text{VTEC}}{NmF_2} \quad (7)$$

and it can be considered a measurement of the inverse of the shape of the electron density profiles at the  $F_2$  layer

**Fig. 5** Colocated vertical profiles of electron density derived from FORMOSAT-3/COSMIC observables over Ascension Island on January 8, 2007. For each occultation, the figure caption indicates the LEO and GPS satellites involved and the occurrence time. Separability has been used to derive these profiles and those of Fig. 6

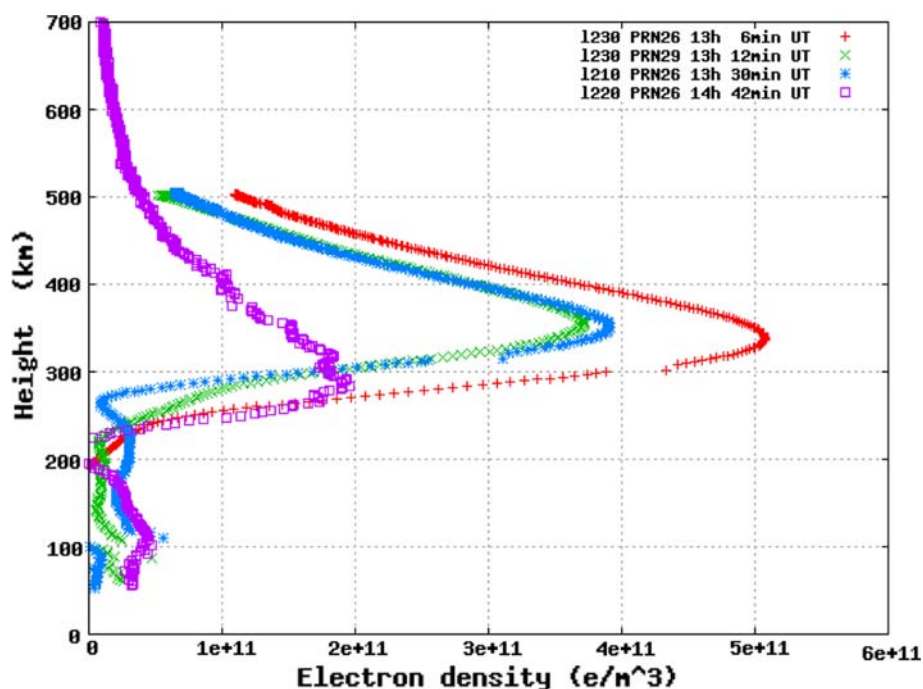
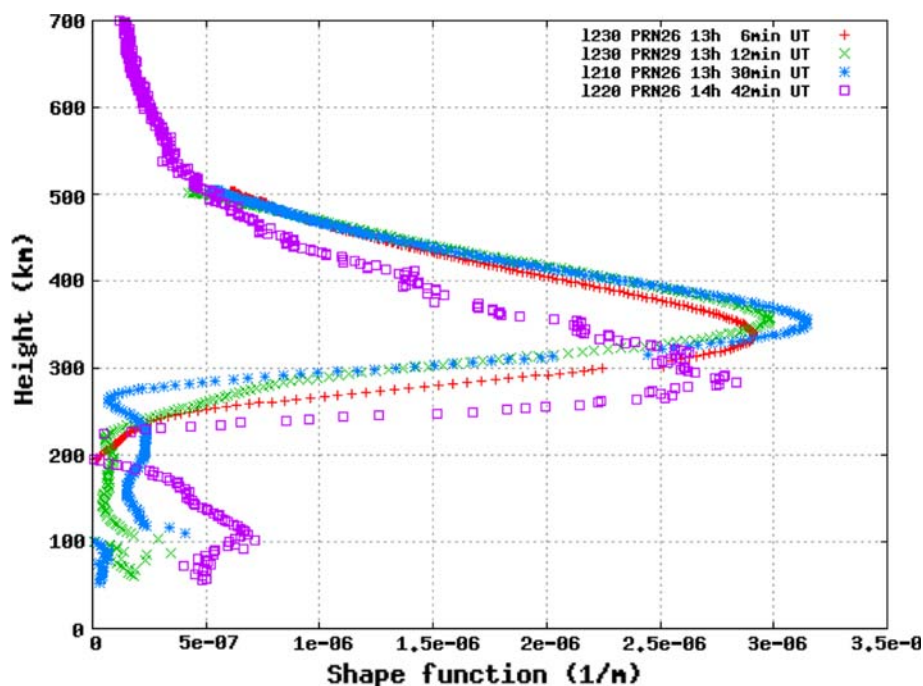


**Fig. 6** Shape functions corresponding to colocated vertical profiles of electron density derived from FORMOSAT-3/COSMIC observables over Ascension Island shown in Fig. 5



peak when solved from radio occultation data using separability. To take an electron density profile as valid, the corresponding slab thickness value is calculated and a threshold for slab thickness is applied. After studying the dependency of the slab thickness as function of the local time for the analyzed period, values below 175 km and above 800 km are discarded. In this sense, the consistency between ionosonde values of  $f_oF2$  and computed VTEC has been checked. Once filtered by slab thickness, accepted

occultations and ionosonde data have been compared with ionosonde measurements, colocated in time and space for comparisons: in time, one hour centered at the epoch that the occultation took place and, in space, a maximum colocation distance of 2000 km has been considered. Since the subpoints of an ionospheric occultation are scattered over large distances (for a LEO satellite of height  $h = 800$  km the maximum length of the occultation region is about 3000 km), the colocation is considered at the ray

tangent point with maximum electron density, i.e., maximum frequency  $f_oF2$ .

## Results

A comparison between retrieved parameters from radio occultations and ionosonde measurements is presented. First, we discuss the use of calibrated and non-calibrated data for occultations in the Ascension Island region. Then the global results are shown for frequency and height estimations.

### Frequency comparisons: $F2$ layer

Manually calibrated data from Ascension Island ionosonde (code name AS00Q) made possible an intercomparison of radio occultations  $f_oF2$  derived frequencies from calibrated and non-calibrated data. This allows validating the expected error of ionosonde data. That is to say, a quantification of the difference in data sources has been possible. Note that all the intercomparisons that are presented later for the parameters derived from radio occultations density profiles were carried out with ionosonde data from the SPIDR website that are, in principle, non-calibrated data.

In Fig. 7 the difference of  $F2$  layer critical frequency values between calibrated and non-calibrated ionosonde data is shown as a function of the local time for the analyzed period.

It can be observed that the best agreement is during the daytime (<10%), while the major discrepancies are found

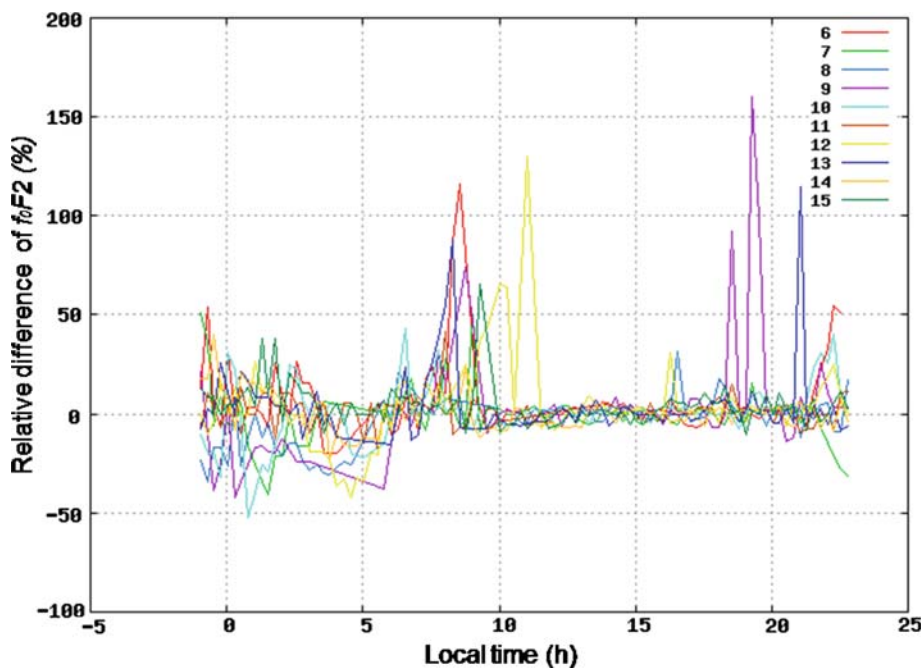
during dusk, dawn and night in agreement with ionosonde worst expected performances.

Figure 8 summarizes the comparison of the performance between the spherical symmetry approach of the classical Abel inversion and the separability approach for non-calibrated ionosonde data (considered as reference truth). The results show that the global performance of the separability approach proof to be 45% better on average for  $f_oF2$  than is the classical Abel transform. Therefore, the introduction of VTEC information when retrieving profiles improves the estimation compared to what is obtained, assuming spherical symmetry. These conclusions are comparable and compatible with previous results (Hernandez-Pajares et al. 2000; Garcia-Fernandez 2004), where the ionospheric combination LI was used. Therefore, the equivalence of using LI or bending angle as main input data for ionospheric inversions is confirmed over these datasets.

### Frequency comparisons: $E$ layer

Regarding the estimation of the  $E$  layer critical frequency  $f_oE$ , the comparison of the classical Abel inversion and the separability implementation has been studied. The  $E$  layer is the ionospheric region, between about 90 km and 150 km that influences long-distance communications by strongly reflecting radio waves in the range of 1–3 MHz. It partially absorbs frequencies above 10 MHz. Davies (1990) notes that the  $E$  layer appears at sunrise and essentially disappears at sunset because the primary source of ionization is no longer present. For this reason,

**Fig. 7** Differences of  $f_oF2$  values in percent versus local time as computed from calibrated and non-calibrated ionosonde data for the period Jan 6–15, 2007



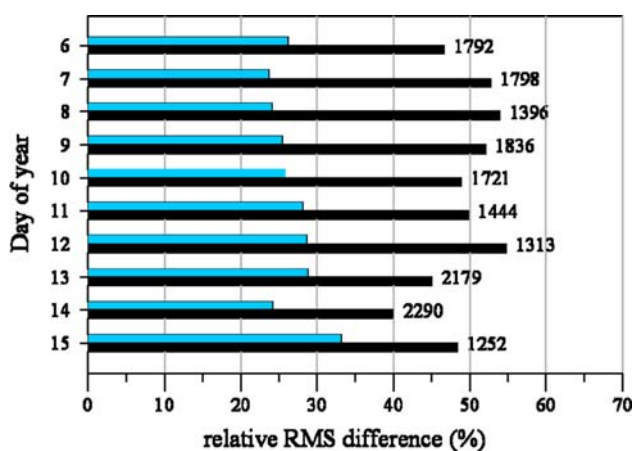


**Fig. 8** Relative RMS differences for the  $F_2$  critical layer frequency comparisons with ionosonde collocation distances up to 2000 km and 1 h time span in local time for the period Jan 6–15, 2007. *Black* and *blue* refer to spherical symmetry and separability, respectively. The numbers of intercomparisons are indicated

the efforts to detect this layer have been restricted to local times spanning 7–17 h, searching electron density profiles for occultations with a peak in the height range 90–150 km. Degradation with respect to the  $f_oF_2$  results is expected due to the recursive nature of the inversion method: the errors are accumulated downward. Hence, the lower, the layer the larger the error in the estimated characteristic parameters. Tables 1 and 2 provide global RMS values for the period analyzed for collocation distances up to 2000 km. The number of comparisons is provided. The average improvement for low latitudes is 32% whereas the average improvement for mid and high latitudes is around 21%.

**Table 1** Low latitude comparison of RMS of  $f_oE$  errors for classical Abel (SPH) and separability (SEP) with respect to ionosonde direct measurements for the data period during daytime

Day of year	Nr. comp.	RMS <sub>SPH</sub> [%]	RMS <sub>SEP</sub> [%]
006	86	1.51 [47.8]	0.77 [24.2]
007	72	1.85 [51.6]	0.91 [25.4]
008	101	1.59 [45.9]	1.13 [32.7]
009	49	1.53 [43.9]	0.88 [25.2]
010	97	1.63 [49.6]	1.19 [36.2]
011	56	1.32 [40.2]	1.26 [38.2]
012	108	1.75 [52.6]	0.92 [27.8]
013	178	1.50 [44.4]	1.25 [37.0]
014	196	1.59 [47.1]	1.15 [34.2]
015	69	1.18 [35.9]	0.62 [19.0]

The error is the absolute RMS expressed in MHz, and the percentage relative RMS difference is provided in brackets. The number of intercomparisons is also included

**Table 2** Mid and high latitude comparison of RMS of  $f_oE$  errors for classical Abel (SPH) and separability (SEP) with respect to ionosonde direct measurements for the data period during daytime

Day of year	Nr. comp.	RMS <sub>SPH</sub> [%]	RMS <sub>SEP</sub> [%]
006	441	0.84 [32.5]	0.99 [38.0]
007	599	1.55 [57.3]	1.36 [50.2]
008	322	1.34 [49.6]	0.88 [32.7]
009	525	1.33 [46.1]	0.93 [32.2]
010	411	1.26 [44.7]	1.15 [40.8]
011	581	1.22 [45.5]	1.03 [38.3]
012	637	1.32 [49.0]	1.03 [38.3]
013	846	1.29 [46.8]	0.96 [34.8]
014	1268	1.24 [47.0]	0.82 [31.2]
015	681	1.21 [46.4]	0.97 [37.4]

The error is the absolute RMS expressed in MHz, and the percentage relative RMS difference is provided in brackets. The number of intercomparisons is also included

### Height comparisons

Empirical equations can be applied to some measured ionospheric characteristics in order to derive  $hmF_2$  values or use  $hmF_2$  from the true-height analysis of ionosonde measurements. For instance, the Shimazaki's relation (Shimazaki 1955) is an empirical formula relating  $hmF_2$  inversely to  $M(3000)F_2$ . The latter represents the ratio of the maximum usable frequency at a distance of 3000 km to the  $F_2$  layer critical frequency. The relation is

$$hmF_{2\text{Shimazaki}} = \frac{1490}{M(3000)F_2} - 176 \quad (8)$$

This formula overestimates heights during daytime under the presence of underlying ionization since that reduces the  $M(3000)F_2$  factor (Shimazaki 1955). Later research, such as Badley and Dudeney (1973) and Dudeney (1983), proposed corrections to (8) by including a dependency on the ratio  $f_oF_2/f_oE$ . A very realistic estimation for  $hmF_2$  is given by the following expression (Dudeney 1983):

$$hmF_{2\text{Dudeney}} = \frac{1490 \cdot F}{M(3000)F_2 - \Delta M} - 176 \quad (9)$$

$$F = M(3000)F_2 \cdot \sqrt{\frac{0.0196 \cdot M(3000)F_2^2 + 1}{1.2967 \cdot M(3000)F_2^2 - 1}} \quad (10)$$

$$\Delta M = \frac{0.253}{\frac{f_oF_2}{f_oE} - 1.215} - 0.012 \quad (11)$$

where  $f_oF_2$  and  $f_oE$  are expressed in MHz. According to these relationships,  $M(3000)F_2$  and the ratio  $f_oF_2/f_oE$  are the driver parameters of Dudeney's  $hmF_2$  approximation. For this study, such parameters have been also extracted

from the SPIDR website. It should be pointed out that the  $E$  layer is mainly a day-time ionospheric layer, basically due to the ionization of the atmosphere caused by solar EUV emission. For this reason, some authors restrict the use of expression in (9) to guarantee reliable results for  $hmF2$ . In this work, the two restrictions imposed in Rishbeth et al. (2000) have been adopted:

- $M(3000)F2 > 2.5$
- $\frac{f_0F2}{f_0E} > 1.7$

These restrictions limit the number of input ionosonde data for which the  $M(3000)F2$  values have acceptable quality (values are especially bad during night time). Because of these restrictions, the intercomparisons are only provided for daytime. Tables 3 and 4 summarize the results for the height comparisons of the  $f_0F2$  peak for ionosonde data. These results are in agreement with the generally accepted error of the Dudeney formula when applied to ionosonde data (discrepancies of the  $hmF2$  estimation below 30 km (Zhang et al. 1999)).

The discrepancies in the  $hmF2$  determination when using the classical Abel approach are not significant with respect to separability.

## Conclusions

The FORMOSAT-3/COSMIC constellation has provided valuable data sets to explore the feasibility of a new implementation of the separability approach to the classical Abel transform inversion when retrieving electron density profiles from radio occultations. This implementation has been carried out using bending angles as main input data, completing previous works where separability

**Table 3** Low latitude comparison of  $F2$  layer critical peak height as derived from FORMOSAT-3/COSMIC radio occultations and Dudeney formula for the data period during daytime

Day of year	Nr. comp.	Bias [km]	$\sigma$ [km]
006	240	-05.85	20.0
007	214	06.31	12.9
008	245	-18.10	19.5
009	162	14.80	17.4
010	157	18.75	16.1
011	80	25.11	18.4
012	129	12.45	20.5
013	202	-10.98	26.1
014	247	-10.69	17.4
015	114	-07.04	21.0

The results show bias and standard deviation  $\sigma$  for the separability approach versus ionosonde data

**Table 4** Mid and high latitude comparison of  $F2$  layer critical peak height derived from FORMOSAT-3/COSMIC radio occultations and Dudeney formula for the data period during day time

Day of year	Nr. comp.	Bias [km]	$\sigma$ [km]
006	0866	12.13	29.6
007	0680	06.00	25.2
008	0677	10.37	23.4
009	1001	22.72	20.2
010	1053	14.29	26.0
011	1134	06.51	25.5
012	0996	01.70	26.5
013	1709	06.56	33.8
014	1862	05.95	22.2
015	1114	04.57	27.1

The results show bias and standard deviation  $\sigma$  for the separability approach versus ionosonde data

was implemented for the ionospheric combination LI in a very straightforward way that is not possible when using bending angles. In order to apply separability to the bending angle, a set of approximations has been done allowing the bending angle to be expressed in terms of changes of refractive index making this method suitable to be extended to tropospheric occultations. In order to mitigate clock drifts, the equivalence of using the excess phase of the ionospheric free combination  $L_c$  as to double differencing has been shown for ionospheric heights. In this way, indirectly, it has been confirmed that the ray path difference between  $L_1$  and  $L_2$  is not significant, validating the method with LI used in previous research. Regarding height comparisons, the results for  $hmF2$  confirm expected results in previous research that are compatible with the reference error. The global performance confirms the improvement of the separability implementation in Abel inversion (45%) by using the bending angle. The equivalence of the results obtained with bending angle and LI implementing separability have been shown in terms of  $f_0F2$  and  $f_0E$  frequencies and  $hmF2$  heights. This implementation opens the possibility for its extension to neutral atmospheric profiling.

**Acknowledgments** The authors would like to express their gratitude to the University Corporation for Atmospheric Research (UCAR), the National Space Organization (NSPO) in Taiwan for the availability of FORMOSAT-3/COSMIC constellation data, the International GNSS Service (IGS) for making available IONEX files, the source of ionosonde data SPIDR and, Dr. David Altadill at Ebro Observatory for providing calibrated AS00Q ionosonde data. This work has been partially supported by the Spanish Ministry of Science and Technology and the European Social Funds under the program "Personal Técnico de Apoyo", and the IBER-WARTK project ESP2007-62676.

## Appendix

In order to implement separability to bending angles, it would be required to have a proportional relationship between bending angles and electron densities that would allow, for two consecutive concentric spherical layers, to write the increment of bending angles as the corresponding increment of electron densities within the two layers. Unfortunately, this is not the case and some approximations are needed to derive such proportionality. Details are given later.

We start from the definition of the ionosphere's refractive index  $n$  derived by Appleton and Hartree, and accept that it can be approximated by first-order form with an accuracy better than 0.1% (Davies 1990),

$$n^2 = 1 - \frac{f_p^2}{f^2} \quad (12)$$

where  $f$  is the system operating frequency and  $f_p$ , the plasma frequency that is defined by

$$f_p = \sqrt{\frac{N_e \cdot e^2}{\epsilon_0 m (2\pi)^2}} \quad (13)$$

where  $e$  stands for the electron charge,  $\epsilon_0$  the permittivity of free space and,  $m$  the rest mass of an electron. Hence, the expression in (12) now becomes

$$n^2 = 1 - \frac{N_e \cdot e^2}{\epsilon_0 m (2\pi f)^2} \quad (14)$$

Differentiating the latter equation gives

$$2n dn = -\frac{e^2}{\epsilon_0 m (2\pi f)^2} dN_e \quad (15)$$

$$\frac{dn}{n} = -\frac{1}{2\epsilon_0 m (2\pi)^2} \frac{e^2}{(f^2 - f_p^2)} dN_e \quad (16)$$

Considering the nominal value of GPS frequency  $L_1$  ( $f_1 = 1575.42$  MHz) and the plasma frequency ( $f_p = 20$  MHz), the denominator in (16) can be approximated by

$$f^2 - f_p^2 \approx f^2 \quad (17)$$

Substituting (17) into (16) leads to

$$\frac{dn}{n} \approx -\frac{1}{2\epsilon_0 m (2\pi)^2} \frac{e^2}{f^2} dN_e \quad (18)$$

The latter equation provides the key to separability implementation when using the  $L_1$  bending angle  $\alpha_1$  as input data for the inversion since it will give the proportionality relationship between bending angle and electron density.

Using Bouguer's formula, which is equivalent to Snell's law in a spherically symmetric medium, we can

establish the relationship of bending angle  $\alpha$  and the refractive index  $n$

$$nr \sin \theta = a \quad (19)$$

The symbol  $r$  stands for the geocentric distance,  $\theta$  the zenith angle of the LOS vector and  $a$  the impact parameter. Considering a layered ionosphere, the change between different layers is obtained by differentiating (19)

$$\Delta nr \sin \theta + n \Delta r \sin \theta + nr \cos \theta \Delta \theta = 0 \quad (20)$$

Rearranging the terms in previous equation gives

$$\Delta \theta = -\frac{\Delta n}{n} \tan \theta - \frac{\Delta r}{r} \tan \theta \quad (21)$$

The first term in (21) takes into account the change in the ray path due to the changes in the refractive index while the second depends on the geometric variations. Actually, the first term provides the definition of the bending angle change in terms of  $n$ ,

$$\Delta \alpha = -\frac{\Delta n}{n} \tan \theta \quad (22)$$

Recalling the expression in (18), it can be derived that the increment of bending angle between consecutive layers with different refractive index is

$$\Delta \alpha = -\frac{\Delta n}{n} \tan \theta = \frac{1}{2\epsilon_0 m (2\pi f)^2} \Delta N_e \tan \theta \quad (23)$$

Therefore, the total bending angle for one ray path would be obtained by adding all bending angle contributions

$$\alpha = \sum \Delta \alpha_i = \frac{1}{2\epsilon_0 m (2\pi f)^2} \sum \Delta N_{ei} \tan \phi_i \quad (24)$$

## References

- Anthes RA, Bernhardt PA, Chen Y, Cucurull L, Dymond KF, Ector D, Healy SB, Ho SP, Hunt DC, Kuo YH, Liu H, Manning H, McCormick C, Meehan TK, Randel WJ, Rocken C, Schreiner WS, Sokolovskiy SV, Syndergard S, Thompson DC, Trenberth KE, Wee TK, Yen NL, Seng Z (2008) The COSMIC/FORMOSAT-3 mission: early results. Bull Am Met Soc 89:313–333. doi: [10.1175/BAMS-89-3-313](https://doi.org/10.1175/BAMS-89-3-313)
- Badley PA, Dudeney JR (1973) A simple model of the vertical distribution of electron concentration in the ionosphere. J Atmos Terr Phys 35:2131–2146
- Davies K (1990) Ionospheric Radio, Chapter 5, IEE Electromagnetic Waves Series 31, Peter Peregrinus Ltd., ISBN 0 86341 186 X, pp 124–154
- Dudeney JR (1983) The accuracy of simple methods for determining the height of the maximum electron concentration of the F2-layer from scaled ionospheric characteristics. J Atmos Terr Phys 45:629–640
- Garcia-Fernandez M (2004) Contributions to the 3D ionospheric sounding with GPS data, Doctoral Thesis, Technical University of Catalonia (UPC), B.45104-2004/84-688-8156-2

- Hajj GA, Romans LJ (1998) Ionospheric electron density profiles obtained with the global positioning system: results from the GPS/MET experiment. *Radio Sci* 33(1):175–190
- Hajj GA, Ao CO, Iijima BA, Kuang D, Kursinski ER, Mannucci AJ, Meehan TK, Romans LJ, de la Torre Juarez M, Yunck TP (2004) CHAMP and SAC-C Atmospheric occultation results and intercomparisons, *J Geophys Res* 109(D6). ISSN 0148-0227, pp D06109.1–D06109.24
- Hernandez-Pajares M, Juan JM, Sanz J (2000) Improving the Abel inversion by adding ground data LEO radio occultations in the ionospheric sounding. *Geophys Res Lett* 27:2743–2746
- Hernandez-Pajares M, Juan JM, Sanz J, Orus R, Garcia-Rigo A, Feltens J, Komjathy A, Schaer SC, Krankowski A (2009) The IGS VTEC maps: a reliable source of ionospheric information since 1998, *J Geod*. doi:[10.007/s00190-008-0266-1](https://doi.org/10.007/s00190-008-0266-1)
- Lei J, Syndergaard S, Burns AG, Solomon SC, Wang W, Zeng Z, Roble RG, Wu Q, Kuo YH, Holt JM, Zhang SR, Hysell DL, Rodrigues FS, Lin CH (2007) Comparison of COSMIC ionospheric measurements with ground-based observations and model predictions: preliminary results. *J Geophys Res* 112:A07308. doi:[10.1029/2006JA012240](https://doi.org/10.1029/2006JA012240)
- Rishbeth H, Sedgemore-Schulthess KJF, Ulich Th (2000) Annual and semiannual variations in the height of the ionospheric F2-layer. *Ann Geophys* 18(3):285–299
- Schaer S, Gurtner W, Feltens J (1998) IONEX: the IONosphere Map EXchange. Format Version 1, Proceedings of the 1998 IGS Analysis Centres Workshop, ESOC, Darmstadt, Germany, Feb 9–11, pp 233–247
- Schreiner S, Sokolovskiy SV, Rocken C, Hunt DC (1999) Analysis and validation of GPS/MET in the ionosphere. *Radio Sci* 34(4):949–966
- Schreiner S, Sokolovskiy SV, Rocken C, Hunt DC (2008) Quality assessment of GPS radio occultation data from the COSMIC/FORMOSAT-3, CHAMP, GRACE missions, FORMOSAT-3/COSMIC 2008 Workshop, Taipei, Taiwan, Oct 1–3
- Shimazaki T (1955) World-wide daily variations in the height of the maximum electron density of the ionospheric F2-layer. *J Radio Res Lab (Japan)* 2(7):85–97
- Wickert J, Reigber Ch, Beyerle G, König R, Marquardt C, Schmidt T, Grunwaldt L, Galas R, Meehan TK, Melbourne WG, Hocke K (2001) Atmosphere sounding by GPS radio occultation: first results from CHAMP. *Geophys Res Lett* 28:3263–3266
- Wickert J, Beyerle G, Hajj GA, Schwieger V, Reigber Ch (2002) GPS radio occultation with CHAMP: Atmospheric profiling utilizing the space-based single difference technique, *Geophys Res Lett* 29(8), doi: [10.1029/2001GL013982](https://doi.org/10.1029/2001GL013982)
- Zhang SR, Fukao S, Oliver WL (1999) Data modeling and assimilation studies with the MU radar. *J Atmos Terr Phys* 61:563–583